Solar Cell Operating Point for Joint LiFi Communication and Harvesting in Battery-Free Devices

Javier Talavante, *Graduate Student Member, IEEE*, Borja Genoves Guzman, *Senior Member, IEEE,* Domenico Giustiniano, *Senior Member, IEEE*

***Abstract*—Solar cells have shown promising performance for Simultaneous Lightwave Information and Power Transfer (SLIPT). Most of literature has focused on applying this concept to battery-powered high-data rate communication. Nevertheless, its application is also particularly advantageous in the low-data rate regime for battery-free systems. However, we find that using the same solar cell causes both communication and harvesting performances degradation. This problem is particularly critical in battery-free systems for its size and power constraints. This paper reveals that the reason behind this problem is that solar cells are typically operated at their Maximum Power Point (MPP), which optimizes energy harvesting but is inefficient for communication. In order to address this finding we introduce, for the first time, the Maximum Communication Point (MCP), a new operating point that complements the traditional MPP by optimizing communication performance. We then propose a transformer-based SLIPT design that enables an accurate control of the impedance at the solar cell's output and thereby allowing precise selection of its operating point. Extensive experiments show that our system provides communication gains of 5x in peak-to-peak received voltage when operating at the MCP, and harvested power gains of more than 3x when operating at the MPP, with respect to the best performing state-of-the-art design.**

***Index Terms*—Battery-free, energy harvesting, Internet of Things (IoT), Light-Fidelity (LiFi), Simultaneous Lightwave Information and Power Transfer (SLIPT), solar cell.**

I. Introduction

Battery-free communication has been proposed as a solution to the threat caused by the usage of batteries in massive deployments of Internet of Things (IoT) devices [1]. Batteries have a short lifetime, and are currently largely based on metals such as Lithium and Cobalt. These metals are difficult to extract, can be found only in a few regions of the planet, and have a significant harmful environmental impact, especially at the time of their disposal. Without the battery, wireless devices operate solely on *harvested energy*, significantly reducing their carbon footprint in their whole life cycle.

The concept of battery-free communication has extended beyond radio frequency (RF) to include optical technologies. In fact, Light-Fidelity (LiFi), which uses modern artificial light sources for communication, can also benefit from battery-free operation. On the transmitter side, LiFi technology leverages the pervasive deployment of retrofitted light-emitting diodes (LEDs) for optical wireless communication. On the receiver side, two types of optical devices are usually considered: photodiodes, optimized for communication, and solar cells, optimized for energy harvesting.

Photodiodes typically require power-hungry active amplifiers with consumption in the order of mW [2]. However, battery-free systems are designed to operate with peak power consumption from a few to hundreds of μW depending on the use case [3]. Besides, photodiodes are more prone to saturation under strong background light, requiring more complex signal processing techniques to effectively receive data [4]. On the contrary, solar cells perform entirely passively due to their large photosensitive area and can better tolerate high background light. Besides, light energy harvesting with solar cells has stood out among other energy sources because of its high efficiency [5]. Overall, a single solar cell can be used for both energy harvesting and data reception, leading to the so-called Simultaneous Lightwave Information and Power Transfer (SLIPT) concept, which enables the design of optical battery-free systems.

However, LiFi technology is typically deployed indoors, where solar cells perform suboptimally due to their poor efficiency under artificial lighting. This inefficiency is caused by the mismatch between the spectral response of solar cells and artificial lighting spectrum, in addition to the low indoor optical power levels. As a result, solar cells harvest less energy than when operating outdoors. This calls for innovative electronics designs to maximize the harvested power indoors. This has been traditionally alleviated with commercial and off-the-shelf (COTS) energy harvesters that automatically adjust the solar cell operating point to the maximum power point (MPP) [6]. While the spectral mismatch remains, those inefficiencies are minimized when operating at MPP, as it ensures extracting the maximum possible power from the solar cell.

When an additional communication branch is introduced after the solar cell to perform SLIPT, we find in this work that operating at the MPP is no longer guaranteed, resulting in performance degradation of both communication and harvesting. As a consequence, we identify the following two challenges for using solar cells in battery-free SLIPT systems:

- **Challenge 1 - Low 3-dB bandwidth of solar cells**: the large capacitance of solar cells limits the achievable data rate. So far, the research community put efforts in maximizing the energy harvested by solar cells, but

The work at IMDEA Networks has been funded in part by the European Union's Horizon 2020 research and innovation program under grant agreement No 101016411 H2020. The work at IMDEA Networks and Universidad Carlos III de Madrid have been funded in part by TUCAN6-CM (TEC-2024/COM-460), funded by CM (ORDEN 5696/2024). Borja Genoves Guzman has also received funding from the European Union under the Marie Skłodowska-Curie grant agreement No 101061853.

Javier Talavante and Domenico Giustiniano are with IMDEA Networks Institute, Leganes, Madrid 28918 Spain. Borja Genoves Guzman is with Universidad Carlos III de Madrid, Department of Signal Theory and Communications, Leganes, Madrid 28911 Spain. Javier Talavante is also with Universidad Carlos III de Madrid. E-mails: javier.talavante@imdea.org, domenico.giustiniano@imdea.org, bgenoves@ing.uc3m.es

ignored the implications of using the same approach also for SLIPT systems;
- **Challenge 2 - Trade-off between communication and harvesting**: In SLIPT systems, the signal received by the solar cell must be used for both communication and energy harvesting. Ideally, the Direct Current (DC) component should feed the harvester, and the alternating current (AC) the communication receiver. However, we find that prior battery-free designs have failed to achieve this ideal split of DC and AC components.

In order to address the aforementioned challenges, we present the first battery-free IoT device that maximizes the communication performance rather than the harvesting performance. In terms of the design space, optimizing the communication performance requires maximizing peak-to-peak signal output voltage. In our study, we show that this peak-to-peak voltage strongly depends on the solar cell's operating point and how the MPP negatively impacts it. We comprehensively study the performance of the solar cell to maximize the voltage difference between the highest and lowest signal level (e.g. for on-off keying (OOK) modulation) and, unlike the MPP commonly used in the literature, for the first time we derive a maximum communication point (MCP) to maximize the communication performance.

To ensure the stable operation of the solar cell at MCP, it is essential to tackle two issues. First, we need to set the operating point so that the system can achieve the maximum data rate in LiFi downlink. We propose to address this issue by invoking the MPP tracking system of commercial harvesting integrated circuits (ICs), but we leverage it for computing the percentage of open circuit voltage at which the solar cell achieves its maximum data rate. Second, we need to control the impedance at the solar cell output accurately, as we deploy one branch for communication and another for harvesting. In this work, we find that traditional resistor-capacitor (RC) circuits are not sufficient to address this issue. Therefore, we propose to adopt a transformer-based SLIPT design that maintains the desired impedance for both communication and harvesting branches.

Our main contributions can be summarized as follows.

- We propose an operating point for solar cells, called MCP, that maximizes the peak-to-peak voltage of the received LiFi signal. It allows reaching communication rates that were not possible before, even under very strong background light conditions, enabling its deployment in a large variety of light conditions;
- We propose a design for the IoT device that can efficiently handle both energy harvesting and communication. It is based on a transformer design that efficiently splits the DC and AC parts of the received signal for harvesting and communication, respectively. This allows us to accurately control the desired operating point of the solar cell output to maximize both operating modes.

The rest of the paper is structured as follows: In Section II we present a review of the existing literature relevant to our proposed solution. In Section III we present the motivation of our study and the fundamentals of the solar cell model when performing SLIPT. Section IV addresses the first challenge by introducing the MCP discovered to maximize the communication performance. In Section V, we address the second challenge by presenting our SLIPT system design and we compare it to the state of the art. Section VI shows the evaluation of our design and its benefits in terms of data rate, range and robustness against background light. Section VII evaluates the autonomy and achievable data rate when our concept is applied to an IoT device installed on an actual greenhouse scenario, further assessing the proposed solution under realistic conditions. Finally, we conclude the paper in Section VIII.

II. Related work

Relationship Between SLIPT and SWIPT in Wireless Systems. SLIPT can be seen as the optical version of the so-called Simultaneous Wireless Information and Power Transfer (SWIPT) in RF systems [7]. In SWIPT, power from RF waveforms is converted to DC for energy harvesting. The growing interest in this technique has led to optimization of the design of the transmitted waveform to enhance the DC power at the output of the rectenna [8] and improve the energy harvesting. However, the actual usage of these systems is hindered by the fact that RF energy distribution is not homogenous in free-space [9] and by the lower conversion efficiency of radio frequency to power with respect to light [10].

Splitting Techniques in Optical Wireless Systems: Space, Time, and Power. In optical wireless systems, LiFi communication and energy harvesting functionalities can be split between a dedicated photodiode and a solar cell [11]. This space-splitting schemes involve certain drawbacks, such as less efficient space usage on the device. In [12], a photodiode equipped with the necessary shielding to prevent saturation occupies nearly a quarter of the area allocated to solar panels. We note that, using this area for additional solar cells, the device could potentially generate up to 25% more energy. This consideration is particularly relevant for battery-free IoT devices, where constraints exist not only on power availability, but also on weight and size. Regarding power consumption, authors in [13] implement a receiver chain that accounts for close to one third of the total consumption of the device, required due to the use of a photodiode as a receiver. Time-splitting is also possible to tackle this matter [14], but again incurs in energy losses by dedicating time to energy harvesting or data reception exclusively. Unlike time- and space-splitting techniques, power-splitting allows performing both tasks simultaneously with the same optical component, increasing the efficiency in both tasks. However, most of the SLIPT systems using solar cells still require costly and power-expensive components [15]–[17].

Deployment Scenarios and Optimization of LiFi-based SLIPT Systems. A typical deployment scenario of LiFi systems consists of retrofitting indoor LEDs for communication. These LEDs provide the dual functionality of transmitting data and illuminating simultaneously. Besides, due to the small cells created by each light bulb, the interference received by the user device is minimal in comparison to traditional RF

communications. This fact is important for IoT, as it simplifies the IoT receiver that is power- and complexity-constrained. Several works have focused on optimizing different aspects of this type of deployment. This scenario offers multiple possibilities to leverage the high density of transmitters and the small size of the cells, such as resource allocation [18], beamforming [19], optimization of transmitted power of the LEDs [20], or usage of intelligent reflecting surfaces [21]. Moreover, optimizing SLIPT becomes especially valuable when a hybrid LiFi/RF system is used, as harvested power may enhance the RF performance in terms of data rate [22], resource allocation [23], [24], and balancing energy harvesting against consumption [25], [26]. This research area also opens opportunities to thoroughly investigate the characteristics of solar cells used simultaneously as data receivers and energy sources. In the experimental domain, guidelines for prototyping LiFi for IoT applications by using an open-source platform are given in [27]. Some works exploited LiFi transmitters also as a source of energy, which may lead to battery-free IoT devices [6], [28]–[30]. However, all these works did not optimize the receiver design and can detect the LiFi signal only under very favorable conditions, i.e. short distance and low background light.

Challenges for Efficient SLIPT. The first challenge presented in Section I has been addressed in prior works by acting over different elements of the LiFi system. Some systems deliver a large amount of energy to the device by transmitting LiFi communication using laser diodes. This operation enables higher data rates and longer distances, as these devices can be pulsed at higher frequencies (MHz) and do not scatter the light [15], [31]. However, this alternative invokes power-intensive electronics on the receiver side for filtering, amplification and equalization, increasing power consumption to hundreds of mW. The low 3-dB bandwidth offered by solar cells can be slightly increased by operating them in reverse bias, at the expense of reducing the overall power conversion efficiency [32], [33]. While solar cell models are based on receiving a DC light signal, very few works tried to model the solar cell when receiving an AC signal for communication along with the DC component [34].

The second challenge presented in Section I motivates the need for splitting both AC and DC components of a LiFi received signal. The low-power optical IoT notion leads to focusing on extracting energy to harvest from the DC component, which will be more abundant in scenarios with background light. Also, the above-mentioned energy harvesters are DC-DC converters, which perceive the AC component as a disturbance. This need has been tackled in prior work by Pareto-optimal solutions to maximize energy harvested and data reception [6], [30]. This solution is based on traditional RC filters that split the received signal power in a DC branch for energy harvesting, and an AC branch for data reception. However, we find in this work that the solution is not able to control accurately the impedance after the solar cell, as the RC filters dissipate power that reduces the receiver efficiency.

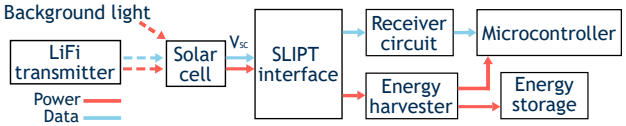

Fig. 1: Block diagram of a SLIPT system using a solar cell both as a LiFi data receiver and energy harvester. The SLIPT interface splits the solar cell signal output V_{SC} for data reception and energy harvesting.

III. Motivation and System Model

This section motivates our study. After introducing the system model, we elaborate on the equivalent circuit of a solar cell, and how such circuit model and its operation at the MPP affects the communication performance in a SLIPT system.

An example of a SLIPT system is shown in Fig. 1, where we show the management of power and data signals and their interconnection in a block diagram. The scenario we aim to study involves two different light sources: one with both AC and DC components from a LiFi transmitter, and one with only a DC component from background light, such as sunlight. The incident power from both sources on the solar cell generates a current at the receiver which can be described as:

$$I_{\mathrm{ph}} = \eta\,(P_{\mathrm{bck}} + P_{\mathrm{tx}} \cdot H), \tag{1}$$

where I_{ph} is the instantaneous photogenerated current in the solar cell, η is the responsivity of the solar cell, P_{bck} is the optical power from all background light sources impinging onto the solar cell, P_{tx} is the transmitted optical power, and H represents the LiFi channel model from the LiFi transmitter to the solar cell. In this paper we aim to optimize the signal reception in the solar cell for simultaneous communication and energy harvesting, based on the photogenerated current I_{ph}. Since we focus on the instantaneous current, the time dependence of P_{tx} can be omitted without loss of generality.

A. Solar cell model

Conceptually, a solar cell receives optical power and converts it into a current I_{ph} with a linear proportional conversion. Besides, the solar cell voltage V_{SC} and solar cell current I_{SC} depend on the optical power received and, consequently, on the current I_{ph} generated. The relationship between V_{SC} and I_{SC} is typically expressed through the current-voltage curves. They are pivotal for the computation of the output power from such solar cell, formulated as $P_{\mathrm{SC}} = I_{\mathrm{SC}} \cdot V_{\mathrm{SC}}$. We can maximize P_{SC} by operating the solar cell at its MPP voltage, i.e., when $V_{\mathrm{SC}} = V_{\mathrm{MPP}}$ the maximum power transfer is ensured. To compute the V_{MPP} of a solar cell, it is key to determine a theoretical solar cell model that matches the real behaviour.

1) Current-voltage curve of a solar cell

Solar cells performing as elements to harvest light energy have been studied for decades. Several works have modeled solar cells to study parameters such as the fill factor or the quantum efficiency that maximize the energy harvested [35], [36], this way enhancing the solar cell manufacturing process and the circuitry behind it. These studies resulted in well-defined electrical models that are suitable to perform under a

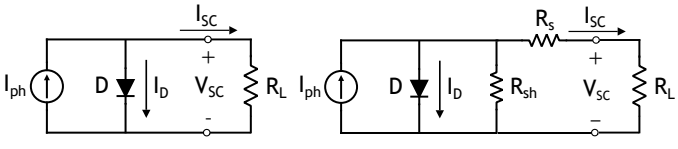

(a) Ideal model. (b) Non-ideal model.

Fig. 2: Models of solar cell under DC illumination.

non-modulated light, i.e. received DC optical power. Typically, the solar cell operation is modeled under DC illumination conditions because sunlight does not exhibit sharp variations, but instead changes gradually throughout the day. We can find two main DC solar cell models in the literature:

Ideal model [37]: The simplest equivalent circuit of a solar cell under DC illumination is a source generating a current $I_{\rm ph}$, in parallel with a diode D through which a current $I_{\rm D}$ circulates. This diode models the limitation of the solar cell to produce a current output as $V_{\rm SC}$ increases. This equivalent circuit is shown in Fig. 2a, being the equation of the output current $I_{\rm SC}$:

$$I_{\rm SC} = I_{\rm ph} - I_{\rm D}. \tag{2}$$

Considering an ideal diode, $I_{\rm D}$ can be modeled as [37]:

$$I_{\rm D} = I_0\,(e^{qV_{\rm SC}/(nkT)} - 1), \tag{3}$$

where I_0 is the saturation current of the diode, q is the electron charge, n is the recombination index, k is Boltzmann constant and T is the junction temperature. Among these, only I_0, n and $I_{\rm ph}$ are intrinsic parameters that define the solar cell, and they are related to its composition.

Non-ideal model [38]: A more complex model explains the behaviour of solar cells more accurately by also accounting for their parasitic effects. These effects are modeled by parasitic series ($R_{\rm s}$) and shunt ($R_{\rm sh}$) resistances shown in Fig. 2b. Following this model, the output current is:

$$I_{\rm SC}=\frac{R_{\rm sh}(I_{\rm ph}+I_0)-V_{\rm SC}}{R_{\rm sh}+R_{\rm s}} - \frac{n_{\rm cell}nkT}{R_{\rm s}q}\times W_0\left[\frac{R_{\rm sh}R_{\rm s}I_0q}{n_{\rm cell}nkT(R_{\rm sh}+R_{\rm s})}\cdot\exp\left(\frac{(R_{\rm sh}R_{\rm s}(I_{\rm ph}+I_0)+R_{\rm sh}V_{\rm SC})q}{n_{\rm cell}nkT(R_{\rm sh}+R_{\rm s})}\right)\right], \tag{4}$$

where W_0 is the principal branch of the Lambert W function and $n_{\rm cell}$ is the number of cells in series connected between both terminals.

A comparison of the two theoretical models with respect to experimental measurements when a solar cell is illuminated with an artificial white light is depicted in Fig. 3. This figure shows the differences between $I_{\rm SC}$-$V_{\rm SC}$ curves obtained with the ideal and the non-ideal models. Parameter values of the ideal and non-ideal theoretical models have been determined by least-squares method to approach experimental measurements.[1] We observe that the current output from the solar cell ($I_{\rm SC}$) is almost constant up to a certain $V_{\rm SC}$ value, which is the threshold voltage of diode D. Above that, $I_{\rm SC}$ starts decreasing to zero current produced at the open-circuit voltage $V_{\rm OC}$.

[1]Those values are: I_0=150.9 nA and $n = 2$ for the ideal model; I_0=107.8 nA, $n = 2$, $R_{\rm s} = 82\,\Omega$, and $R_{\rm sh}$=5.31 kΩ for the non-ideal model; fixing $n_{\rm cell} = 4$ and $T = 298$ K.

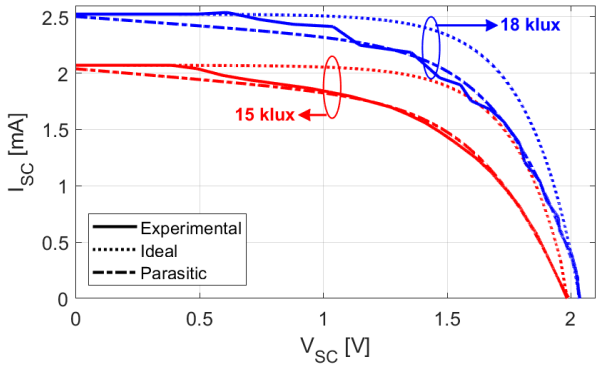

Fig. 3: $I_{\rm SC}$-$V_{\rm SC}$ curves for the same solar panel under two different illuminances: 15 klux (blue) and 18 klux (red). Non-ideal solar cell model provides a better fit.

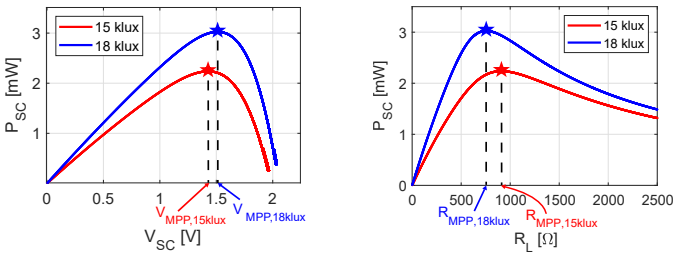

(a) $P_{\rm SC}$ vs. $V_{\rm DC}$ (b) $P_{\rm SC}$ vs. $R_{\rm L}$

Fig. 4: Harvested power curves of the solar cell under two different illuminances computed with the non-ideal solar cell model. The maximum power voltage operating point ($V_{\rm MPP}$) or the external load setting it ($R_{\rm MPP}$) is different for each light level.

While the ideal solar cell model provides a totally flat $I_{\rm SC}$ until the threshold voltage of diode D, the effects of the parasitic resistances in the non-ideal model induces a slight decreasing slope at low voltages. Note that the non-ideal solar cell model matches very well with the experimental measurements, which shows its great accuracy to model the solar cell behaviour at DC. From now on, we assume a non-ideal model in our study.

2) Power harvested by a solar cell

The received DC signal is maximized when the solar cell operates at its MPP denoted by $V_{\rm MPP}$. This is achieved by modifying the load connected at the solar cell output $R_{\rm L}$, which ensures a maximum power transfer. As an example, Fig. 4 depicts both $P_{\rm SC}-V_{\rm SC}$ and $P_{\rm SC}-R_{\rm L}$ curves for the two different received illuminances included in Fig. 3. Curves show a global maximum (MPP), highlighted with a star marker. However, such MPP is obtained at $V_{\rm MPP}$ and $R_{\rm L}$ values that vary according to the incident luminous flux, i.e., they change according to the $I_{\rm SC}-V_{\rm SC}$ curve of the solar cell. Therefore, a system that automatically adapts to lighting conditions is needed to maintain the solar cell operating at $V_{\rm MPP}$.

This issue was solved in prior works by MPP tracking (MPPT) systems, which dynamically adapt the voltage in the

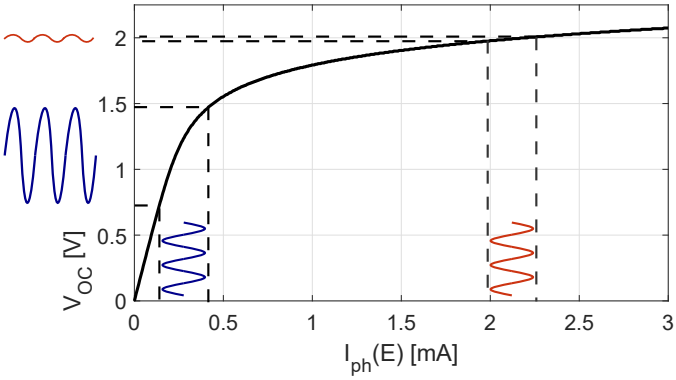

Fig. 5: Voltage AC response of a solar cell under AC and DC incident illuminance. The logarithmic dependence of $V_{\rm SC}$ induces a decrease in the AC amplitude with the increase of the DC light component.

solar cell output to extract the maximum available power from it, regardless of changes in light conditions [39], [40]. MPPT systems are typically applied to non-constrained designs using large areas of photovoltaic panels. However, simpler techniques suitable for low-cost and low-power chips can achieve the same objective with sufficient precision.

One of the most widespread approaches is the *constant voltage method*. In this method, the energy harvesting circuit disconnects the solar cell from the load $R_{\rm L}$ for a small amount of time and samples its open circuit voltage $V_{\rm OC}$, by charging up a capacitor or through an analog-to-digital converter (ADC). Then it fixes the output voltage of the solar cell at a percentage of this $V_{\rm OC}$, where $V_{\rm MPP}$ is expected to be found, which is usually between 70% and 85%. This input can be sampled periodically and implemented with a simple control loop to dynamically adapt to the DC current level [39]. Due to its simplicity, it is the one used by most of the COTS compact energy harvesters.

This energy harvester is an IC that is usually connected directly to an energy source like a solar cell, and includes an MPPT circuit to hold the MPP of this energy source in this port. These ICs include a connection for the energy storage device, e.g., a supercapacitor. They charge it through a voltage converter between the energy source and the storage, which is adaptive since the voltage input changes. The stored energy is used to provide constant voltage in a different port. Therefore, *the harvester IC provides a stable voltage for powering up the rest of the device*.

B. Maximum power point (MPP) is detrimental for LiFi communication

As shown above, operating the solar cell at its MPP means to introduce a positive voltage across the solar cell connectors, then ensuring a maximum power transfer. Differently, it has been demonstrated that maximizing the received AC signal for communication is attained by reducing the solar cell internal capacitance, which is achieved by reducing the operating voltage to a negative bias [32]. These two operation points are conflicting. A trivial solution to this problem is to dedicate two different solar cells, one optimized for DC and the other for AC. However, this approach leads to a greater complexity, a higher energy consumption,[2] and a larger form factor that is prohibitive for IoT devices.

The AC voltage output of a solar cell can be directly connected to an ADC. Extracting the AC signal in this scenario can be performed with passive circuitry in the receiver, so no extra power is required. Demodulating an output voltage signal from a solar cell involves some issues that are studied in the following. Without loss of generality, let us assume that we operate in open-circuit ($I_{\rm SC}=0$) and with the non-ideal solar cell theoretical model (see Section III-A). Looking at its $V_{\rm OC}-I_{\rm ph}$ representation in Fig. 5, the main issues of decoding a voltage-modulated signal outputting from a solar cell are the logarithmic dependence and the DC level, which are discussed in what follows.

Logarithmic dependence. Solar cell output voltage has a logarithmic dependence on the incident light through $I_{\rm ph}$. Non-linearities have always been a severe limitation for data communication, as they lead to amplitude and phase distortions of the received signal.

DC level. The DC component of the received light power influences the performance of a voltage-based decoder. In LiFi systems, $I_{\rm ph}=I_{\rm DC}+I_{\rm AC}(t)$. $I_{\rm DC}$ is the current produced by background illumination conditions, while $I_{\rm AC}(t)$ is generated by the modulated LiFi source. Then, $I_{\rm DC}$ determines the voltage output offset. Due to the logarithmic dependence shown in Fig. 5, the larger the offset, the smaller the peak-to-peak voltage produced by $I_{\rm AC}(t)$ will be, which dramatically impacts the communication performance. It is difficult to prevent the solar cell from receiving a DC background illumination in LiFi scenarios and, in fact, receiving a DC background illumination is beneficial from an energy harvesting perspective. This trade-off problem must be addressed in the receiver circuitry.

These issues could be overcome with: 1) large-area solar panels to augment the amount of received signal power [17]; 2) powerful and highly-directive LiFi transmitters to transfer more power to the user device [16]; or 3) power-expensive amplifiers to increase the received signal power [45]. However, all these solutions are not suitable for applications where the receiver is size- or power-constrained, which is the case of low-data rate regime in battery-free IoT systems. In the next section, we tackle all the presented issues by designing a novel receiver that implements a maximum communication point.

IV. Maximum Communication Point

This section addresses the first challenge *low 3-dB bandwidth of solar cells* introduced in Section I. As introduced before, the maximum power is extracted from the solar cell if $V_{\rm MPP}$ is maintained at its output, but the operation point for the maximum communication performance has been

[2]Maximizing the AC signal means achieving a photocurrent that is linear with the incident light power, that has a low offset, a low noise and offers a broad bandwidth performance [41]. This is achieved when voltage between the terminals of the photosensitive device remains constant, either in reverse or zero-bias. Maintaining the voltage constant while enabling current variations usually requires a bias circuit and a trans-impedance amplifier (TIA) which is power-hungry for battery-free IoT applications [42]–[44].

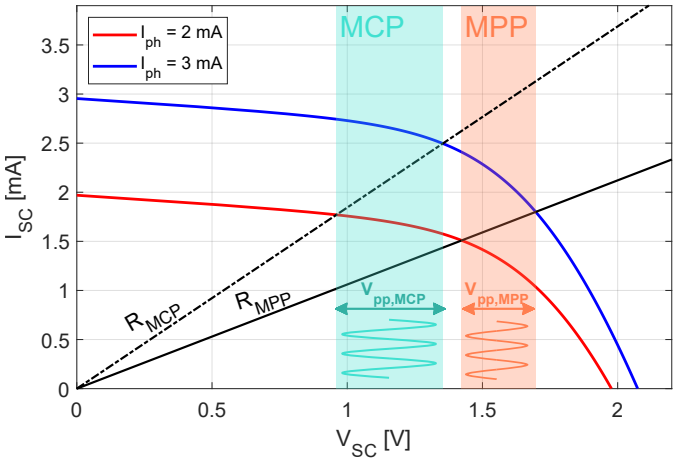

Fig. 6: I-V curves for a solar cell under two illuminance conditions: with background light only (red) and background light plus the 'ON' level of a LiFi signal (blue). The amplitude of the AC voltage response under a LiFi signal is determined by the operating point, being maximum when it is equal to V_{MCP}.

overlooked so far. We propose to optimize the DC output voltage of the solar cell to maximize the peak-to-peak voltage (AC voltage) employed for communication, according to the light levels received from the background DC illumination and LiFi AC signals. We name this new operating point as *Maximum Communication Point (MCP)*, obtained when maintaining V_{MCP} at the solar cell output. In the following we study how such V_{MCP} must be calculated.

This approach is aimed to maximize the peak-to-peak amplitude of the AC voltage signal at the output of the solar cell, named as V_{pp}. It can be observed as an increase in the optical-to-electrical conversion efficiency. This method is agnostic to the modulation scheme and data rate, including those used in high-end LiFi transmitters. Without loss of generality, we consider an OOK modulation scheme where the light is 'ON' to transmit bit '1', and 'OFF' to transmit bit '0'. The received signal produces two $I_{\mathrm{SC}} - V_{\mathrm{SC}}$ curves that must be analyzed to maximize the amplitude of the AC voltage signal V_{pp}:

- One $I_{\mathrm{SC}} - V_{\mathrm{SC}}$ curve when the modulated light source output is 'OFF', i.e., the solar cell receives only the ambient illumination;
- Another $I_{\mathrm{SC}} - V_{\mathrm{SC}}$ curve when the modulated LiFi source is 'ON', i.e., the solar cell receives both ambient and modulated lights.

These two $I_{\mathrm{SC}} - V_{\mathrm{SC}}$ curves are represented in Fig. 6. When bit '1' is transmitted, $I_{\mathrm{ph}} = 3\,\mathrm{mA}$, and when bit '0' is transmitted, $I_{\mathrm{ph}} = 2\,\mathrm{mA}$. The load impedance seen from the solar cell R_{L} determines the operating voltage V_{SC}. In Fig. 6, this impedance is represented by a straight line with its origin at (0,0) coordinates and slope $\frac{1}{R_{\mathrm{L}}} = \frac{I_{\mathrm{SC}}}{V_{\mathrm{SC}}}$. The difference between the voltage values at which this line intersects both $I_{\mathrm{SC}} - V_{\mathrm{SC}}$ curves is the V_{pp} generated after the solar cell. Note that the R_{L} value is pivotal for the V_{pp} maximization. As an example, Fig. 6 plots the V_{pp} obtained when operating at MCP and MPP, providing $V_{\mathrm{pp,MCP}}$ and $V_{\mathrm{pp,MPP}}$, respectively.

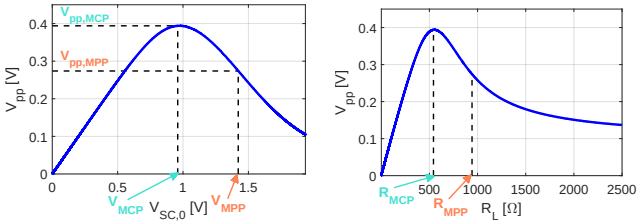

(a) (b)

Fig. 7: Theoretical V_{pp} response of the solar cell for (a) a range of voltage operating points or, equivalently, (b) the load impedance R_{L}, with highlighted responses for MCP and MPP.

We observe an amplitude gain when operating at MCP with respect to the MPP. If background illumination is negligible, we would have only one $I_{\mathrm{SC}} - V_{\mathrm{SC}}$ curve and the largest V_{pp} would be achieved at open-circuit. However, when the background light is significant, the MCP must be computed by considering the two $I_{\mathrm{SC}} - V_{\mathrm{SC}}$ curves generated. This is the main difference with respect to the computation of the MPP operating point explained in Section III, which requires only one $I_{\mathrm{SC}} - V_{\mathrm{SC}}$ curve as it only considers the DC level of the received signal.

Let us name $V_{\mathrm{SC},0}$ as the operating voltage when the solar cell receives bit '0' and $V_{\mathrm{SC},1}$ the one when bit '1' is received, both for the same R_{L}. Figure 7 shows $V_{\mathrm{pp}} = V_{\mathrm{SC},1} - V_{\mathrm{SC},0}$ as a function of $V_{\mathrm{SC},0}$ and the corresponding R_{L}. Both plots indicate the existence of an optimal value of $V_{\mathrm{SC},0}$ or R_{L} that maximizes V_{pp} and, therefore, the communication capabilities of the solar cell with low-power circuitry. This solar cell operating point is the MCP, named as V_{MCP}, and it changes for every two $I_{\mathrm{SC}} - V_{\mathrm{SC}}$ curves produced when modulating a LiFi source with a background DC light. Note that these values of $V_{\mathrm{SC},0}$ and R_{L} do not correspond to the MPP, also depicted. Given the shape of the power curves shown in Fig. 4, there is a trade-off between optimizing communication and energy harvesting governed by the solar cell operating point.

Under the condition $V_{\mathrm{SC}} = I_{\mathrm{SC}} \cdot R_{\mathrm{L}}$, we can see that Eq. (4) becomes a transcendental equation in V_{SC}. Consequently, it is not possible to obtain a closed-form expression for V_{pp} from which the MCP could be derived analytically. Instead, a method to obtain it is to sweep R_{L} in its possible range and determine the optimal R_{L} value that provides the maximum V_{pp}, as depicted in Fig. 7. However that is time- and power-consuming and would deprive the device of receiving data during the process. In the following section we introduce a SLIPT design that allows controlling the R_{L} impedance accurately to exploit this novel MCP concept, together with the MPP. This design allows maximizing both the energy harvesting and the communication while using passive circuitry elements that minimizes the IoT tag power consumption.

V. SLIPT SYSTEM DESIGN

This section addresses the second challenge *trade-off between communication and harvesting* introduced in Section I, while maintaining the MCP discovered in Section IV. A SLIPT system requires that both energy harvesting and communication are performed simultaneously, and we must evaluate how

operating the solar cell at V_{MPP} and V_{MCP} points affect the performance of both tasks.

A. Setting up the Maximum Power Point (MPP) and Maximum Communication Point (MCP) at indoor IoT scenarios

Setting up the MPP: The setting of the load impedance leading to the MPP is commonly ensured by making the solar cell operating at a voltage that is fixed as a percentage of the V_{OC}, then leading to the V_{MPP}. Setting up this constant percentage has a great advantage as it can be implemented in a simple IC with few external components. It allows harvesting energy close to the maximum levels without requiring complex circuitry that sweeps the $I_{\mathrm{SC}} - V_{\mathrm{SC}}$ curve, computational resources to perform time-series calculations, memory to store temporal data or temperature compensation systems. For that reason, assuming V_{MPP} as a percentage of V_{OC} and providing a system to hold it is the preferred method when implementing efficient solar energy harvesting in IoT devices.

Nevertheless, as we showed in Fig. 3 and Fig. 4, different values of I_{ph} (i.e. different incident light) lead to different V_{MPP} values that may not correspond to a fixed percentage of the V_{OC}. This variation has drawn the attention of a significant part of the photovoltaic community to research solar cells performing indoors [46] [47].

We aim at showing the variability of the MPP operating point and at quantifying its harvested power loss. In this way, we will determine if holding the percentage of V_{OC} is suitable for IoT. We connect a potentiometer to the output of a solar cell acting as load R_{L}. Solar cell used is an IXOLAR SM111K04L [48]. We illuminate the solar cell with six different levels of illuminance: 3, 6, 9, 12, 15 and 18 klux[3], ensuring the light level with a luxmeter EXTECH Model SDL400. At these six illumination conditions, we find the MPP by tuning R_{L} searching for the resistance maximizing the power transfer. Fig. 8a shows the results obtained in this experiment, where we can see a slight increasing tendency with the same slope for all curves. Fig. 8b shows the percentage of V_{OC} at which the MPP is obtained for all illuminance levels, which is calculated from Fig. 8a values. We see that the percentage of V_{OC} that determines V_{MPP} is not constant for all illuminance levels, but the variations produced are negligible. Then, we decide to hold $V_{\mathrm{MPP}} = 0.71 \cdot V_{\mathrm{OC}}$, which is the averaged percentage value of V_{OC} obtained for all illuminance levels in the range of interest.

Setting up the MCP: We aim at exploiting the simple and energy-efficient mechanism shown in Section V-A for the MCP. This means that we aim at discovering a percentage of V_{OC} that allows working at the MCP to maximize the communication performance, and also that this percentage of V_{OC} is constant for the whole indoor illuminance range. In this way, we could retrofit the same hardware used on IoT devices to operate a solar cell at the MPP, just by programming the energy harvester to operate at a different percentage of V_{OC}. This leads to savings in complexity of the circuitry design, size and power consumption. Simply by setting up a different

[3]Note that these illuminance levels are common in indoor places, going from reading tasks [49] to smart indoor farming [50].

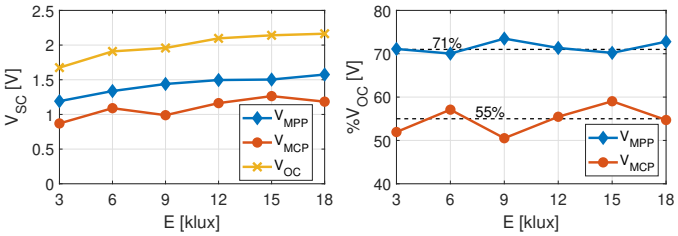

(a) V_{OC}, V_{MPP} and V_{MCP}. (b) Experimental V_{MPP} and V_{MCP} as a percentage of V_{OC}.

Fig. 8: Voltage values at which the MPP and MCP are obtained, and calculation of voltage percentage with respect to V_{OC} at different illuminance levels. MPP is obtained at an averaged $V_{\mathrm{MPP}} = 0.71 \cdot V_{\mathrm{OC}}$, and MCP is obtained at an averaged $V_{\mathrm{MCP}} = 0.55 \cdot V_{\mathrm{OC}}$ for indoor illuminance levels.

R_{L} value for the energy harvester to manage the impedance between the solar cell terminals, we could make the system work at the MCP. However, since the MCP computation relies on two $I_{\mathrm{SC}} - V_{\mathrm{SC}}$ curves rather than one as explained in Section IV, any change in the background or the modulated light may lead to variations of the percentage of the V_{OC}.

Reusing the same setup as before, we transmit a 5 kHz square LiFi signal with the transmitter placed at 35 cm from the solar cell, which translates into an illuminance of 2.07 klux when transmitting bit '1'. While this signal is being received, we tune the potentiometer until finding the maximum V_{pp} and, therefore, the MCP computed as a percentage of the V_{OC}. These results can be seen in Fig. 8a, where we show that, for all indoor illuminance levels, the V_{MCP} slightly increases with the illuminance. Fig. 8b shows the percentage of V_{OC} at which the MPP is obtained for all illuminance levels. We find that the variations observed in the MCP are slightly larger compared to those in the MPP. This increased error is associated to the estimation of two series of I-V, in contrast to the case of MPP, where we must only find the voltage value that maximizes the power output. As this variation of the I-V curves is influenced by the incident light power, in this scenario it is primarily affected by the background light, which is stronger than the AC signal. Considering these sources of uncertainty, we can conclude that $V_{\mathrm{MCP}} = 0.55 \cdot V_{\mathrm{OC}}$, which is the averaged percentage value of V_{OC} obtained for all illuminance levels. Note that V_{OC} is measured every few seconds, which leads to a continuous update in R_{L} to maintain the MCP. This makes the proposed system robust against any potential impact of fluctuations or unevenness in background illumination.

Evaluating the loss produced in MPP: We quantify the loss produced in harvested power when operating at the fixed $V_{\mathrm{MPP}} = 0.71 \cdot V_{\mathrm{OC}}$ in comparison to an optimal varying V_{MPP} value for every illuminance level. To show this, we plot in Fig. 9a the harvested power for all illuminance levels when the solar cell operating point is a varying V_{MPP} and a $V_{\mathrm{MPP}} = 0.71 \cdot V_{\mathrm{OC}}$. The harvested power when operating at an optimal varying V_{MPP} or a $V_{\mathrm{MPP}} = 0.71 \cdot V_{\mathrm{OC}}$ is exactly the same, what concludes that we can set up a fixed 71% of V_{OC} for any indoor illuminance level. Note that this percentage may change for different solar cells and scenarios, so it must be carefully computed before its deployment.

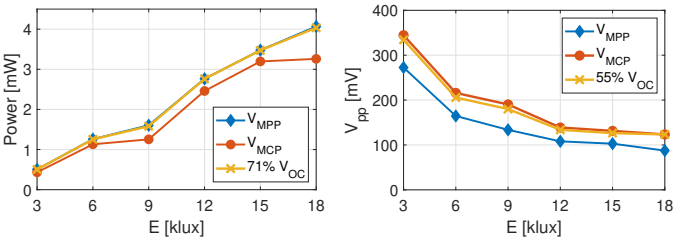

(a) Harvested power for every solar cell operating point.

(b) Communication performance for every solar cell operating point.

Fig. 9: Performance of harvested power and communication at different illuminance levels when operating at MPP, MCP and the averaged voltage percentage with respect to V_{OC}. The solar cell can be operated at a fixed percentage of V_{OC}, as it produces negligible losses in comparison to a varying optimal operating point. Also, we can see the trade-off between energy harvesting and communication, as choosing an optimal operating point for one task decreases the performance in the other one.

Evaluating the loss produced in MCP: Now we quantify the loss produced in communication when the solar cell operating point is a fixed value of $V_{\mathrm{MCP}} = 0.55 \cdot V_{\mathrm{OC}}$, or an optimal varying V_{MCP} value for every illuminance level. Fig. 9b shows the V_{pp} values obtained for every operating point at any illuminance level, and we can see that the difference in V_{pp} produced when operating at a fixed $V_{\mathrm{MCP}} = 0.55 \cdot V_{\mathrm{OC}}$ in comparison to when operating at an optimal varying V_{MCP} is negligible. This means that we can set up a fixed percentage of V_{OC} to perform as MCP. Further optimization of the operating voltage for communication requires increasing the complexity in the device. However, our approach is energy efficient and satisfies the battery-free IoT constraints.

B. Design choices

Now that we have discovered that both MPP and MCP can be computed as a fixed percentage of V_{OC} for all illuminance levels, we must study a SLIPT system design that allows us to accurately hold V_{SC} at the desired operating point.

Including circuitry to extract the AC data signal without hindering the DC signal for energy harvesting is very challenging. This circuitry must always be active, as it will perform as a wake-up system for energy saving. Therefore, it must be extremely low-power and completely passive. In the following, we introduce the best-performing state-of-the-art low-power SLIPT system, we analyze it, and we present a new SLIPT design that overcomes the state-of-the-art system limitations.

1) State-of-the-art RC filter design.

The state-of-the-art SLIPT implementation [6], [30] is represented in Fig. 10. We use this design as a baseline for our study. It separates both the AC and DC signals dedicated for data reception and energy harvesting, respectively, through two passive RC filters. It can be implemented with very small, passive and non-expensive components, favoring low-power and miniaturized designs. However, its performance notably degrades in presence of a strong background light. Under these

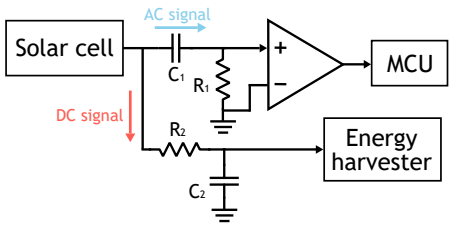

Fig. 10: Baseline RC filters-based passive SLIPT interfaces.

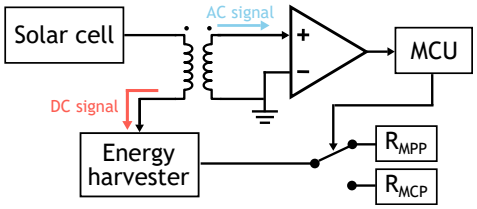

Fig. 11: Proposed transformer-based passive SLIPT interface.

conditions, the current through the resistor in the low-pass filter (R_2) induces a voltage between the solar cell positive terminal and the energy harvester input introducing important power losses.

First, the current through the resistor dissipates power, reducing the energy transferred into the harvester. As the solar cell output current increases with illuminance, the power loss increases accordingly. Second, this positive voltage displaces the voltage operating point of the solar cell. The MPP tracking system of the energy harvester is designed to hold the estimated V_{MPP} at its input, which assumes it is the energy source output (i.e. the solar cell). However, in this RC filter design there is an element with a positive voltage in between. The voltage between the solar cell terminals V_{SC} is the estimated V_{MPP} plus the voltage drop at R_2 denoted by $V_{\mathrm{R_2}}$: $V_{\mathrm{SC}} = V_{\mathrm{MPP}} + V_{\mathrm{R_2}}$. This voltage increase moves the operating point of the cell away from the MPP in the x-axis of the curve shown in Fig. 3. Therefore, the solar cell is not really operating at its MPP. In this region, a small increase in the voltage largely decreases the power that the solar cell can transfer. Also, this problem aggravates with the value of the resistor as shown in [6], [30]. A higher resistance leads to a significant voltage increase with the same solar cell current, shifting the voltage operating point away from the MPP and increasing power losses.

2) Proposed transformer-based design.

Our proposal uses a transformer to extract the data signal from the solar cell, allowing all the output current from the solar cell to pass into the energy harvester. Transformers have been largely used for separating DC and AC signals in the IEEE 802.3 standard for Ethernet, and have been in part investigated for high-speed communication invoking lasers [51]. We apply this concept here for the first time for energy harvesting and LiFi data reception in battery-free devices with conventional LED-based lighting scenarios. The design is shown in Fig. 11. Note that if high data rates are desired, alternative photoelectronics designs may be necessary. These would include circuitry with larger bandwidth and

Common components	
Solar module	IXOLAR SM111K04L [48]
Energy harvester	e-peas AEM10330 [53]
Comparator	TS881 [54]
Switch	MAX4528 [55]
MCU	MKL03Z32VFK4 [56]

RC filter design		Transformer design	
R_1, C_1	21 kΩ, 10 nF	Transformer	Hammond
R_2, C_2	variable, 10 μF		101F [57]

TABLE I: Components for the passive SLIPT interface.

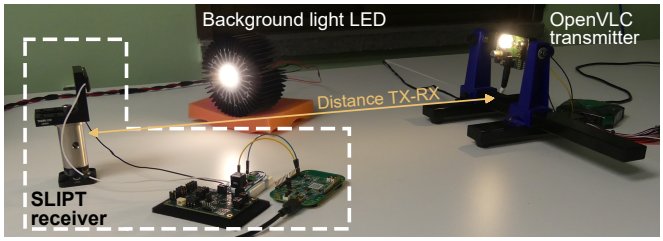

Fig. 12: Experimental setup of the SLIPT system.

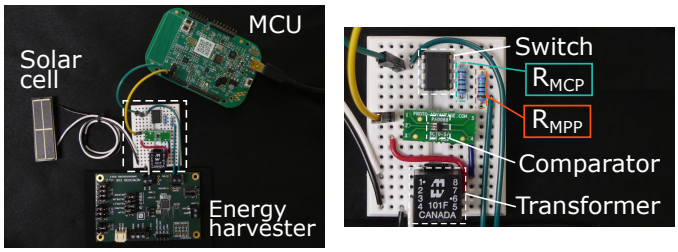

Fig. 13: SLIPT receiver proposed.

larger energy consumption, powered either by batteries or directly from the power grid. In order to achieve the proposed tasks, the bandwidth of the transformer must be sufficient to avoid attenuating the data signal at the secondary side. This bandwidth can be expressed as [52]:

$$BW = \frac{1}{\sqrt{(\frac{L_l}{R_c})^2 + (RC)^2}} - \frac{R_{L_m}}{2\pi L_m}, \tag{5}$$

where L_l is the leakage inductance of the secondary winding, R_c is the core parallel equivalent resistance, C is the parasitic capacitance at the output, R the load resistance, $R_{L_m} = R_c||(R + R_s)$, where R_s is the parasitic series resistance on the secondary winding, and L_m is the magnetizing induction on the secondary side. All these parameters depend on the transformer design and can be designed to fit our circuit. This freedom on designing and tuning the bandwidth of a transformer involves that the main bandwidth limitation comes from the solar cell. Given the large amount of applications where transformers are used, it is feasible to find a COTS model that fits our requirements.

The main benefit from this system is that it avoids the above-mentioned problem: the real impedance from the primary inductor between the solar cell and the harvester is negligible and it does not produce any significant deviation from the desired solar cell operating voltage V_{SC}. In this way, we have a perfect control over the V_{SC} in the solar cell terminals. We can easily manage it by a switch connected to two possible resistive loads that lead to the MPP and MCP operating points, named as R_{MPP} and R_{MCP}, maximizing the power transfer and the communication performance, respectively.

In this paper we experimentally compare the performance of both designs in a SLIPT system that aims to operate at MCP or MPP. To this end, we implement both solutions and compare their performance. This is detailed in the next section.

VI. Experimental results

A. Implementation of SLIPT designs

We implement the baseline and the proposed SLIPT systems depicted in Fig. 10 and Fig. 11, respectively, with off-the-shelf components introduced in Table I. The *solar module* is the IXOLAR SM111K04L [48]. This is a module of four silicon solar cells in series, reaching an open-circuit voltage of 2.76 V at light conditions of 1 sun and providing a maximum power of 98 mW. It has an active area of 6.02 cm^2, making it suitable for small form factors.

The integrated circuit to perform as *energy harvester* is the AEM10330 from e-peas Semiconductors [53]. This chip is an integrated energy management circuit that simultaneously supplies the device and manages the energy storage. It offers the possibility of setting the voltage operating point at any desired percentage of the V_{OC} by means of setting a R_{L} in the solar cell output. This provides significant flexibility to perform at MCP, MPP or any other operating point.

The communication branch is connected to a comparator TS881 [54] to collect the received data. The switch to manage the load at the solar cell output is the MAX4528 [55], and the low-power MCU selected to sample and decode bits is the MKL03Z32VFK4 [56]. Regarding the *SLIPT interface*, we use the following components for each design:

- RC filter design: For the AC branch, we configure C_1 and R_1 at 10 nF and 21 kΩ, respectively, which ensures a cut-off frequency of 757 Hz. The DC branch is composed of a C_2 =10 μF and a varying R_2 for joint energy harvesting and communication optimization [6], [30].
- Proposed Transformer-based design: We use the audio transformer 101F from Hammond [57]. It offers a flat frequency response from 200 Hz to 100 kHz, which achieves larger frequencies than the 3-dB solar cell bandwidth. The volume of this component is close to 1 cm^3, which is still below the characteristic dimension of the solar cell. The form-factor of this transformer could be further reduced by employing a planar transformer. Also, the power rating of the one used here is two orders of magnitude higher than the input power expected from this solar cell.

On the transmitter side, we use the open-source and open-hardware OpenVLC1.3 platform [27]. This is a versatile LiFi platform for IoT applications which can be modulated up to 1 MHz (larger than the solar cell bandwidth). The setup is shown in Fig. 12, where we can see the LiFi transmitter, SLIPT receiver and two of the variables of study: background light and transmitter-receiver distance. A detailed prototype of

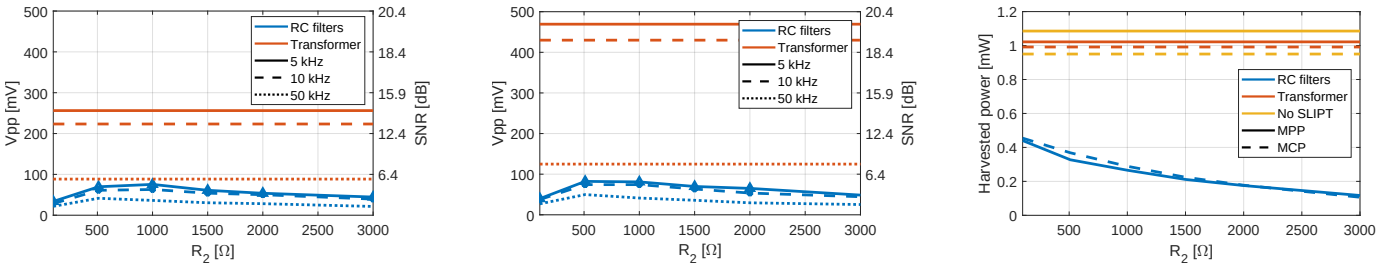

(a) V_{pp} at MPP. (b) V_{pp} at MCP. (c) Power at MPP & MCP.

Fig. 14: Comparison between SLIPT circuits at different voltage operating points. Background light: 6 klux.

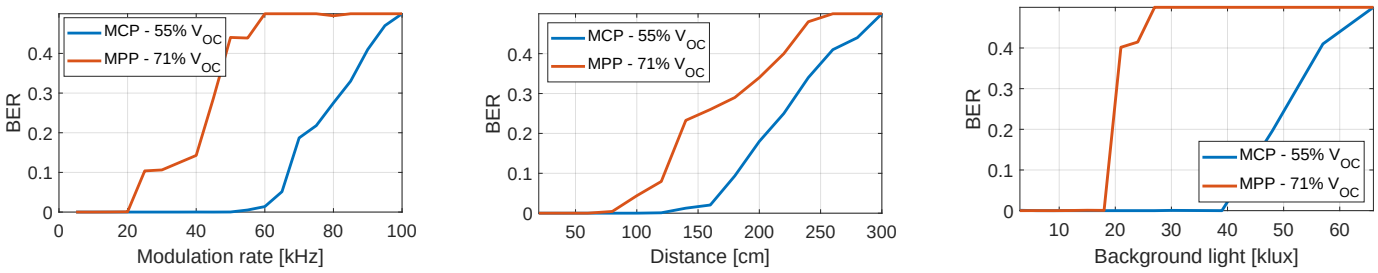

(a) LiFi modulation rate (Distance: 35 cm. Background light: 6 klux).

(b) Distance (Rate: 10 kHz. Background light: 6 klux).

(c) Background light (Rate: 10 kHz. Distance: 35 cm).

Fig. 15: Comparison between the operation of the SLIPT interface at the MPP and MCP.

our proposed SLIPT receiver is represented in Fig. 13, which shows all the components described in Table I.

B. Comparison between the SLIPT designs

We evaluate the performance of our proposed SLIPT design and compare it with the RC design, considering the received V_{pp} and the harvested power as performance metrics. Since the R_2 value in the RC filter design impacts on the balance between communication and energy harvesting, we evaluate the results for a whole range of R_2 values, containing R_{MPP} and R_{MCP}. Then, we compare them to the performance given by our proposed SLIPT system. We create a setup such that the background received light is 6 klux. We transmit a LiFi signal with OOK modulation and measure the voltage received signal before the comparator. Then we evaluate the V_{pp} and harvested power obtained when the energy harvester is configured to perform at MPP or at MCP.

Results are plotted in Fig. 14. Generally, the lower the LiFi rate, the larger the V_{pp} due to lower impact of the solar cell's intrinsic capacitance. In Fig. 14a and Fig. 14b we observe that our proposal outperforms the RC filter design for the whole R_2 range. These plots also show the translation into the voltage signal-to-noise ratio (SNR) at the receiver output, computed as the ratio between the squared V_{pp} and the voltage output noise from the solar cell under background light only. This means that, even performing a Pareto optimization as in [6], [30], our system provides a better performance. The reason is that the R_2 in the RC filter design increases the operating voltage of the solar cell, then making it not to operate at its MPP or MCP, and also dissipating an extra power due to the current going through it as observed in Fig. 14c. Operating at MCP, our system provides a V_{pp} that is 5x larger than the one obtained with the state-of-the-art RC design. Operating at MPP, our system provides a harvested power that is 3x larger than the one obtained with the RC design, achieved at low R_2 values. Also, the V_{pp} from the transformer SLIPT under the MCP duplicates the one obtained when operating at the MPP, which shows the importance of the discovered maximum communication operating point. In Fig. 14c we observe that our proposed transformer-based SLIPT system provides a harvested power very close to a system without SLIPT, regardless of the voltage operating point.

We conclude that the transformer-based design offers a better performance in a SLIPT design than the baseline design. Therefore, we will consider it for the next section, where we will show the experimental performance of the solar cell operating point, studying the proposed MCP to maximize the communication performance in detail.

C. Comparison between MCP and MPP

The gain in the V_{pp} of the signal provided by the proposed MCP translates into an increase of the capabilities of our SLIPT receiver. The working setup is the same as in Fig. 12.

1) Achievable LiFi modulation rate.

First, we evaluate the maximum LiFi modulation rate at which our transformer-based MCP system may decode bits at a low bit error rate. We assess this by increasing the frequency of an OOK LiFi signal for both MPP and MCP operating points. Figure 15a shows that, when operating at the MPP, a zero BER is achieved at 20 kHz, while we can go up to almost 60 kHz when using the MCP with a BER=0. The larger the LiFi modulation rate, the larger the BER is due to the inherent low-pass filter produced by the internal solar cell capacitance.

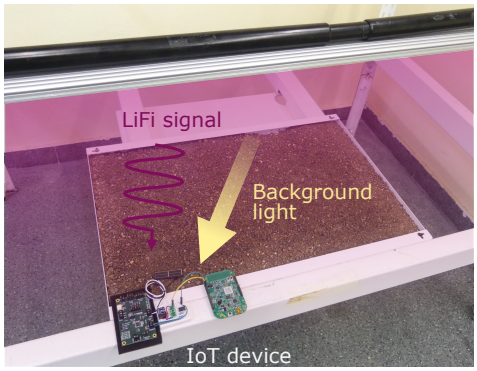

Fig. 16: Deployment of the IoT device in indoor farming for precision monitoring.

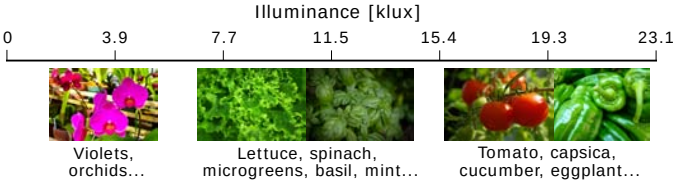

Fig. 17: Illuminance in klux required for different cultivations (for comparison, indoor lighting for user comfort requires about 500 lux). Derived from [50].

2) Achievable distance.

Second, we evaluate the maximum distance at which our transformer-based MCP receiver can effectively decode data. The larger the distance, the lower the optical power received, which reduces the communication performance and leads to many decoding errors as shown in Fig.15b. Note that our proposed transformer-based MCP receiver is able to achieve a larger distance than the transformer-based MPP receiver. For a BER=0.1, we obtain a range increase of 75%.

3) Achievable background light of operation.

Operating under strong background light for the communication IoT device is desired because it would allow harvesting more energy which may lead to operating the IoT devices without traditional power sources. The expected loss in communication performance produced by background illumination could also be compensated by the operation at MCP. Fig 15c shows the BER performance under different background light when operating at a LiFi modulation rate of 10 kHz at a transmitter-receiver distance of 35 cm. We can see the robustness of our proposed transformer-based MCP receiver, that achieves a BER=0 at a maximum background light of 40 klux. Note that this background light is the one that we can find in vertical farming [50], which means that our proposed transformer-based MCP receiver opens the door to operate in real applications.

VII. Greenhouse Application

The good communication performance obtained with our proposed SLIPT design working at the proposed MCP complements the performance in energy harvesting obtained with the traditional MPP. This calls for an adaptive system implemented in the IoT device to switch between MCP and MPP depending on its needs. Besides, the proposed SLIPT design allows adjusting the solar cell load very accurately, and we can control the solar cell voltage to work at MPP or MCP. In this section we test this adaptive design introduced in Fig. 11 under actual greenhouse conditions.

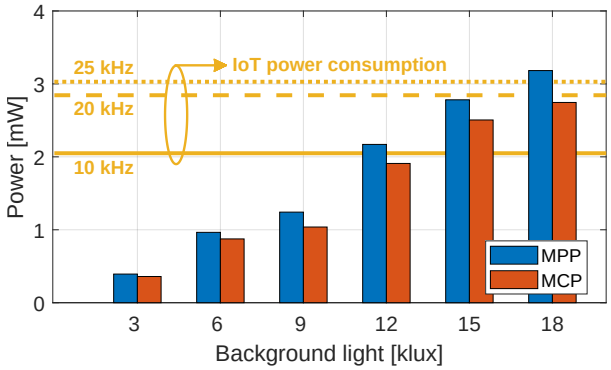

Fig. 18: Harvested power for different background light levels, and comparison with the power consumption for the MCU operating at different demodulation rates.

Indoor farming invokes high-power LEDs to optimize the crop growth, and requires a dense network of sensors deployed in the greenhouse that can monitor the environmental conditions such as humidity, temperature, CO_2 levels, soil moisture, etc. This can be attained with IoT devices, but they must operate without batteries to avoid chemical contamination, reduce labour and maintenance costs to replace batteries, avoid outages, etc. Different works have tested the feasibility of powering up a network of IoT devices with ambient light, either natural sunlight [58] or artificial [59]. In [60], it is shown that when the energy buffer provided by a supercapacitor is sufficiently large, these devices can perform their monitoring tasks at an acceptable frequency, despite the changes in available ambient light during the day. However, these prior works do not consider the downlink communication to these battery-free devices.

Fig. 16 shows our system deployed in a shelf suitable for vertical farming with realistic lighting conditions. Note that indoor farming can grow plants requiring low background light, such as violets, orchids, etc., or plants requiring very high background light such as cucumber, capsica, eggplant or tomatoes. We evaluate our system when operating at a wide range of background lighting covering the needs of a large variety of plants, as depicted in Fig. 17.

We first analyze the harvested power under different background light going from 3 klux to 18 klux, when the IoT device operates at MPP or MCP. Results are plotted in Fig. 18. The larger the background light, the larger the harvested power is. As expected, operating at MPP slightly increases such harvested power in comparison to the MCP. In the same figure, we also include the power consumption of the IoT device for the components listed in Table I, demodulating at 10, 20 and 25 kHz.[4] These are the available frequencies at which the MCU can operate at its low-power mode. Note that the power

[4]The code used for the experiments is available at: https://doi.org/10.5281/zenodo.16786287.

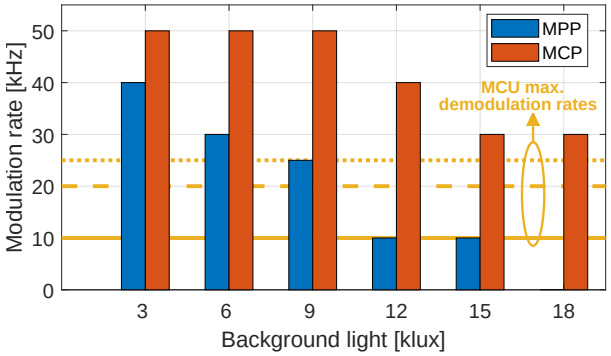

Fig. 19: Maximum modulation rate allowed by the SLIPT system (without MCU) for different background light levels.

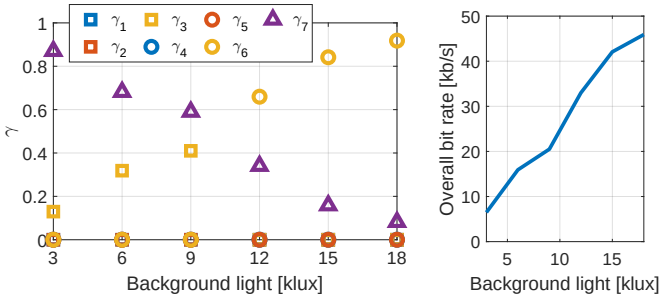

(a) Ratio of time operating at each mode given by γ_m.

(b) Overall maximum bit rate.

Fig. 20: Maximum data rate achieved by the battery-free IoT device for each background light.

consumed by the MCU dominates over the rest of components, as the comparator and switch only consume 1.32 μW and 3.3 μW, respectively. When this power consumption is larger than the harvested one, the IoT device must operate in a duty cycle to activate and deactivate the communication mode.

Fig. 19 plots the maximum modulation rates to achieve a BER equal to zero with a LiFi signal of 2.55 klux when transmitting '1'. Note that the larger the background light, the lower the maximum communication rate. This is due to the lower V_{pp} achieved as expected from Fig. 5. Also, the experiments confirm that operating at MCP allows achieving larger communication rates than operating at MPP. Nevertheless, the IoT device decodes at its maximum demodulation rates of 10 kHz, 20 kHz or 25 kHz, even if the SLIPT design would allow larger values under the evaluated lighting conditions.

We can process the results obtained in Fig. 18 and Fig. 19 to get the maximum overall rates achieved by the IoT device at every background light level. We identify 7 operation modes for the IoT device: 1) MPP with MCU at 10 kHz, 2) MPP with MCU at 20 kHz, 3) MPP with MCU at 25 kHz, 4) MCP with MCU at 10 kHz, 5) MCP with MCU at 20 kHz, 6) MCP with MCU at 25 kHz and 7) MPP without reception (consumption=0 mW). Each of them has a harvested power and power consumption depicted in Fig. 18, and a maximum LiFi modulation rate given by Fig. 19, limited by the maximum demodulation rates supported by the MCU.

We can formulate a linear problem to optimize the ratio of time operating at each mode, defined by $\gamma_m \in [0, 1]$, where $m \in \{1, 2, ..., 7\}$ is the operation mode, with the objective of maximizing the overall data rate r:

$$\max_{\gamma_m \forall m \in \{1,2,...,7\}} \quad \sum_{m=1}^{6} r_m \cdot \gamma_m \tag{6}$$

$$\text{s.t.} \quad \sum_{m=1}^{7} \gamma_m = 1; \sum_{m=1}^{7} P_m \cdot \gamma_m \leq \sum_{m=1}^{7} H_m \cdot \gamma_m;$$

$$\gamma_m \geq 0; \quad \forall m$$

where r_m is the bit rate at mode m that can be 0, 20, 40 or 50 kb/s when demodulating at 0, 10, 20 or 25 kHz rates, respectively. P_m is the power consumed by the IoT device at mode m and H_m is the power harvested at mode m.[5]

Results are shown in Fig. 20a. To maximize its battery-free communication rate, the IoT device operates in only three modes: Modes 3 and 7 under low-background light conditions (3–9 klux), and Modes 6 and 7 under high-background light conditions (12–18 klux). This implies that the IoT device always communicates at its maximum achievable rate of 25 kHz, using Modes 3 and 6, and alternating with Mode 7,[6] which is dedicated solely to energy harvesting. This largely simplifies the overall system as the IoT device has the knowledge to decide when to switch between MPP (Modes 3 and 7) and MCP (Mode 6), and with data decoding (Mode 3) or only harvesting energy (Mode 7). This avoids implementing an uplink communication to inform about the IoT device status and implement a costly system to adapt the LiFi data rate.

Fig. 20b represents the results of the optimization problem that maximizes the overall bit rate. We can see that the larger the background light, the higher the bit rate that can be achieved as the IoT device can harvest energy while receiving data. Our system can achieve an overall LiFi bit rate of around 46 kb/s at a background light of 18 klux.

Apart from smart farming, our system can be applied to multiple indoor and outdoor scenarios. In indoor scenarios, home automation would largely benefit from battery-free IoT systems deployed at large scale and communicating with retrofitted light bulbs. Our approach would address the problem that most of these IoT devices are energy-intensive and dependant on batteries. In outdoor scenarios, deploying IoT sensors opens up a wide range of applications. For instance, large-scale sensor deployments can support the realization of smart cities. Such applications demand extensive sensor networks capable of transmitting data over considerable distances. Our system is well-suited for these scenarios, as outdoor environments often include lighting infrastructure that can be adapted for joint LiFi communication and energy harvesting.

VIII. Conclusion

We have presented a novel SLIPT design to optimize both the communication and energy harvesting performance in

[5]Note that linear programming problems are convex and can be easily solved by any convex solver such as the CVX tool of MATLAB [61].

[6]Switching between modes can be performed with an external instruction provided from the LiFi transmitter. Alternatively, the MCU can sample periodically the solar cell output to estimate the available light energy and expected signal loss, and then switch between MPP and MCP.

battery-free systems. We have discovered a maximum communication point (MCP) that maximizes the voltage amplitude of the received signal. Our MCP provides 2.5x gain in LiFi modulation rate, 1.5x in distance, and it maintains communication without bit errors with more than 2x stronger background illuminance with respect to the traditional MPP. Our SLIPT design allows controlling accurately the solar cell load, and we propose an adaptive solution to make it operate either in the MCP or MPP according to the current IoT status. Our design outperforms the best performing state-of-the-art design in both communication and energy harvesting capabilities. We have extensively evaluated our system, and we have tested it in greenhouse conditions. Our system is able to operate in battery-free mode under background lighting conditions encompassing a large variety of crops. It can achieve up to 46 kb/s at 18 klux.

REFERENCES

[1] S. Ahmed *et al.*, "The Internet of Batteryless Things," *Commun. ACM*, vol. 67, no. 3, p. 64–73, Feb. 2024.

[2] Ismayana, D. R. Utomo, and P. Nugroho, "A comparative study of transimpedance amplifier (TIA) topologies for visible light communication (VLC)-based Internet of Things (IoT) data communication," in *Proc. 10th IEEE Inf. Technol. Int. Seminar (ITIS)*, Nov. 2024, pp. 344–350.

[3] T. Khan, S. N. K. Veedu, A. Rácz, M. Afshang, A. Hoglund, and J. Bergman, "Toward 6G zero-energy internet of things: Standards, trends, and recent results," *IEEE Commun. Mag.*, vol. 62, no. 12, pp. 82–88, Sept. 2024.

[4] Y.-L. Huang, "Nonlinear saturation behaviors of high-speed p-i-n photodetectors," *J. Lightwave Technol.*, vol. 18, no. 2, pp. 203–212, Feb. 2000.

[5] O. B. Akan, O. Cetinkaya, C. Koca, and M. Ozger, "Internet of hybrid energy harvesting things," *IEEE Internet Things J.*, vol. 5, no. 2, pp. 736–746, 2018.

[6] M. S. Mir, B. G. Guzman, A. Varshney, and D. Giustiniano, "LiFi for low-power and long-range RF backscatter," *IEEE/ACM Trans. Netw.*, vol. 32, no. 3, pp. 2237–2252, June 2024.

[7] V. K. Papanikolaou *et al.*, "Simultaneous lightwave information and power transfer in 6G networks," *IEEE Commun. Mag.*, vol. 62, no. 3, pp. 16–22, Mar. 2024.

[8] B. Clerckx and E. Bayguzina, "Waveform design for wireless power transfer," *IEEE Trans. Signal Process.*, vol. 64, no. 23, pp. 6313–6328, Dec. 2016.

[9] A. Galisteo, A. Varshney, and D. Giustiniano, "Two to tango: hybrid light and backscatter networks for next billion devices," in *Proc. 18th ACM Int. Conf. Mobile Syst. Appl. Services (MobiSys)*, June 2020, p. 80–93.

[10] O. B. Akan, O. Cetinkaya, C. Koca, and M. Ozger, "Internet of hybrid energy harvesting things," *IEEE Internet Things J.*, vol. 5, no. 2, pp. 736–746, Apr. 2018.

[11] J. Liu, G. Faulkner, B. Choubey, S. Collins, and D. C. O'Brien, "An optical transceiver powered by on-chip solar cells for IoT smart dusts with optical wireless communications," *IEEE Internet Things J.*, vol. 6, no. 2, pp. 3248–3256, Nov. 2019.

[12] L. De Groot, T. Xu, and M. Z. Zamalloa, "DroneVLC: Exploiting drones and VLC to gather data from batteryless sensors," in *Proc. 2023 IEEE Int. Conf. on Pervasive Comput. and Commun. (PerCom)*, Mar. 2023, pp. 242–251.

[13] A. Perera, M. Katz, R. Godaliyadda, J. Häkkinen, and E. Strömmer, "Light-based internet of things: Implementation of an optically connected energy-autonomous node," in *Proc. 2021 IEEE Wireless Commun. and Netw. Conf. (WCNC)*, Mar. 2021, pp. 1–7.

[14] K. Xu, Z. Shen, Y. Wang, X. Xia, and D. Zhang, "Hybrid time-switching and power splitting SWIPT for full-duplex massive MIMO systems: A beam-domain approach," *IEEE Trans. Veh. Technol.*, vol. 67, no. 8, pp. 7257–7274, 2018.

[15] S. Das, A. Sparks, E. Poves, S. Videv, J. Fakidis, and H. Haas, "Effect of sunlight on photovoltaics as optical wireless communication receivers," *J. Lightw. Technol.*, vol. 39, no. 19, pp. 6182–6190, Oct. 2021.

[16] I. Tavakkolnia *et al.*, "Organic photovoltaics for simultaneous energy harvesting and high-speed MIMO optical wireless communications," *Light: Sci. & Appl.*, vol. 10, no. 41, p. 41, Feb. 2021.

[17] Z. Wang, D. Tsonev, S. Videv, and H. Haas, "On the design of a solar-panel receiver for optical wireless communications with simultaneous energy harvesting," *IEEE J. Sel. Areas Commun.*, vol. 33, no. 8, pp. 1612–1623, Aug. 2015.

[18] A. M. Abdelhady, O. Amin, A. Chaaban, B. Shihada, and M.-S. Alouini, "Downlink resource allocation for dynamic TDMA-based VLC systems," *IEEE Trans. Wireless Commun.*, vol. 18, no. 1, pp. 108–120, Oct. 2018.

[19] K. W. S. Palitharathna, N. D. Wickramasinghe, A. M. Vegni, and H. A. Suraweera, "Neural network-based optimization for slipt-enabled indoor vlc systems with energy constraints," *IEEE Trans. Green Commun. Netw.*, vol. 8, no. 2, pp. 839–851, 2024.

[20] Y. Guo, K. Xiong, Y. Lu, B. Gao, P. Fan, and K. B. Letaief, "SLIPT-enabled multi-LED MU-MISO VLC networks: Joint beamforming and DC bias optimization," *IEEE Trans. Green Commun. Netw.*, vol. 7, no. 3, pp. 1104–1120, Oct. 2022.

[21] Y. Guo, J. Fan, R. Zhang, B. Chang, D. W. K. Ng, D. Niyato, and D. I. Kim, "Secrecy Energy Efficiency Maximization in IRS-Assisted VLC MISO Networks with RSMA: A DS-PPO Approach," *IEEE Trans. Wirel. Commun.*, pp. 1–1, 2025.

[22] Y. Guo, K. Xiong, Y. Lu, D. Wang, P. Fan, and K. B. Letaief, "Achievable information rate in hybrid VLC-RF networks with lighting energy harvesting," *IEEE Trans. Commun.*, vol. 69, no. 10, pp. 6852–6864, Oct. 2021.

[23] S. Shi, G. Gui, Y. Lin, C. Yuen, O. A. Dobre, and F. Adachi, "Joint beamformer design and power allocation method for hybrid RF-VLCP system," *IEEE Internet Things J.*, vol. 11, no. 5, pp. 7878–7892, Sept. 2024.

[24] T. Tang, L. Shi, Q. Li, and Z. Xiong, "Sustainability-driven resource allocation for SLIPT-assisted hybrid VLC/RF IoT systems," *IEEE Wireless Commun. Lett.*, vol. 13, no. 6, pp. 1765–1769, Apr. 2024.

[25] H. Peng, Q. Li, A. Pandharipande, X. Ge, and J. Zhang, "End-to-end performance optimization of a dual-hop hybrid VLC/RF IoT system based on SLIPT," *IEEE Internet Things J.*, vol. 8, no. 24, pp. 17 356–17 371, May 2021.

[26] A. H. F. Raouf, C. K. Anjinappa, and I. Guvenc, "Optimizing energy-harvesting hybrid VLC/RF networks with random receiver orientation," *IEEE Access*, vol. 12, pp. 147 574–147 588, Oct. 2024.

[27] B. G. Guzman, M. S. Mir, D. F. Fonseca, A. Galisteo, Q. Wang, and D. Giustiniano, "Prototyping visible light communication for the Internet of Things using OpenVLC," *IEEE Commun. Mag.*, vol. 61, no. 5, pp. 122–128, May 2023.

[28] J. Li, A. Liu, G. Shen, L. Li, C. Sun, and F. Zhao, "Retro-VLC: Enabling battery-free duplex visible light communication for mobile and IoT applications," in *Proc. 16th Int. Workshop on Mobile Comput. Syst. and Appl. (HotMobile)*, Feb. 2015, p. 21–26.

[29] X. Xu *et al.*, "PassiveVLC: Enabling practical visible light backscatter communication for battery-free IoT applications," in *Proc. 23rd Annu. Int. Conf. on Mobile Comput. and Netw. (MobiCom)*, Oct. 2017, p. 180–192.

[30] M. S. Mir, B. G. Guzman, A. Varshney, and D. Giustiniano, "PassiveLiFi: Rethinking LiFi for low-power and long range RF backscatter," in *Proc. 23rd Annu. Int. Conf. on Mobile Comput. and Netw. (MobiCom)*, Oct. 2021, p. 697–709.

[31] M. Kong *et al.*, "Toward self-powered and reliable visible light communication using amorphous silicon thin-film solar cells," *Opt. Express*, vol. 27, no. 24, pp. 34 542–34 551, Nov 2019.

[32] W. Lei, Z. Chen, Y. Xu, C. Jiang, J. Lin, and J. Fang, "Negatively biased solar cell optical receiver for underwater wireless optical communication system with low peak average power ratio," *IEEE Photon. J.*, vol. 14, pp. 1–9, Aug. 2022.

[33] W.-H. Shin, S.-H. Yang, D.-H. Kwon, and S.-K. Han, "Self-reverse-biased solar panel optical receiver for simultaneous visible light communication and energy harvesting," *Opt. Express*, vol. 24, no. 22, pp. A1300–A1305, Oct. 2016.

[34] Y. Zhou, A. Ibrahim, M. Muttillo, P. Manganiello, H. Ziar, and O. Isabella, "Bandwidth characterization of c-Si solar cells as VLC receiver under colored LEDs," in *Proc. 8th Int. Conf. Smart and Sustain. Technolo. (SpliTech)*, Aug. 2023, pp. 1–5.

[35] M. Neukom, S. Züfle, S. Jenatsch, and B. Ruhstaller, "Opto-electronic characterization of third-generation solar cells," *Sci. and Technol. of Advanced Mater.*, vol. 19, no. 1, pp. 291–316, Mar. 2018.

[36] M. Hejri and H. Mokhtari, "On the comprehensive parametrization of the photovoltaic (PV) cells and modules," *IEEE J. Photovolt.*, vol. 7, no. 1, pp. 250–258, Jan. 2017.

[37] J. Nelson, *The Physics of Solar Cells*. Imperial College Press, 2003.

[38] S. Pindado *et al.*, "Simplified Lambert W-function math equations when applied to photovoltaic systems modeling," *IEEE Trans. Ind. Appl.*, vol. 57, no. 2, pp. 1779–1788, Jan. 2021.
[39] M. de Brito, L. Sampaio, L. Galotto, G. Melo, and C. Canesin, "Evaluation of the main MPPT techniques for photovoltaic applications," *IEEE Trans. Ind. Electron.*, vol. 60, pp. 1156–1167, Mar. 2013.
[40] M. Hlaili and H. Mechergui, "Comparison of different MPPT algorithms with a proposed one using a power estimator for grid connected PV systems," *Int. J. of Photoenergy*, vol. 2016, pp. 1 728 398–1 728 408, Jun. 2016.
[41] OSI Optoelectronics, "Photodiode characteristics and applications," Tech. Rep., 2007.
[42] R. Saffari, M. Dolatshahi, and S. Zohoori, "A fully-integrated, low-power transimpedance amplifier for 5Gbps optical front-end," in *Proc. 28th Iranian Conf. on Elect. Eng. (ICEE)*, 2020, pp. 1–5.
[43] Y. Takahashi, D. Ito, M. Nakamura, A. Tsuchiya, T. Inoue, and K. Kishine, "Low-power regulated cascode cmos transimpedance amplifier with local feedback circuit," *Electronics*, vol. 11, no. 6, Mar. 2022.
[44] M. T. I. Badal, M. B. I. Reaz, L. S. Yeng, M. A. S. Bhuiyan, and F. Haque, "Advancement of CMOS transimpedance amplifier for optical receiver," *Trans. Electr. and Electron. Mater.*, vol. 20, no. 2, pp. 73–84, Apr. 2019.
[45] J. Fakidis, H. Helmers, and H. Haas, "Simultaneous wireless data and power transfer for a 1-Gb/s GaAs VCSEL and photovoltaic link," *IEEE Photon. Technol. Lett.*, vol. 32, no. 19, pp. 1277–1280, Aug. 2020.
[46] A. A. Goje *et al.*, "Review of flexible perovskite solar cells for indoor and outdoor applications," *Mater. for Renewable and Sustain. Energy*, vol. 13, no. 1, pp. 155–179, Apr. 2024.
[47] M. C. Scharber, "Efficiency of emerging photovoltaic devices under indoor conditions," *Solar RRL*, vol. 8, no. 2, p. 2300811, Nov. 2024.
[48] ANYSOLAR Ltd., "SM111K04L. https://www.anysolar.biz/Gen2," Accessed: 02-04-2025.
[49] "ISO 8995:2002 Lighting of indoor work places," International Organization for Standardization, Geneva, CH, Standard, Mar. 2002.
[50] B. G. Guzman *et al.*, "Toward sustainable greenhouses using battery-free LiFi-enabled Internet of Things," *IEEE Commun. Mag.*, vol. 61, no. 5, pp. 129–135, May 2023.
[51] S. Das, "Photovoltaics as high-speed optical wireless communication receiver," PhD thesis, University of Edinburgh, Edinburgh, UK, Sep. 2021.
[52] N. Kondrath and M. K. Kazimierczuk, "Bandwidth of current transformers," *IEEE Trans. Instr. Meas.*, vol. 58, no. 6, pp. 2008–2016, Jul. 2009.
[53] e-peas Semiconductors., "AEM10330. https://e-peas.com/documents /AEM10330/DS-AEM10330.pdf," Accessed: 02-04-2025.
[54] STMicroelectronics., "Comparator TS881. https://www.st.com/ resource/en/datasheet/ts881.pdf," Accessed: 02-04-2025.
[55] Maxim Integrated Products., "Low-Voltage, Phase-Reversal Analog Switch MAX4528. https://www.analog.com/media/en/technical-documentation/data-sheets/MAX4528.pdf," Accessed: 02-04-2025.
[56] NXP Semiconductors, "Kinetis KL03 32 KB Flash. https://www.nxp.com/docs/en/data-sheet/KL03P24M48SF0.pdf," Accessed: 02-04-2025.
[57] Hammond., "Miniature Audio Potted 101 Series. https://www.hammfg.com/electronics/transformers/audio/101.pdf," Accessed: 02-04-2025.
[58] K. E. Jeon *et al.*, "LuXSensing beacon: Batteryless IoT sensor, design methodology, and field test for sustainable greenhouse monitoring," *IEEE Trans. AgriFood Electron.*, vol. 1, no. 2, pp. 86–98, Aug. 2023.
[59] I. Cappelli *et al.*, "Autonomous IoT monitoring matching spectral artificial light manipulation for horticulture," *Sensors*, vol. 22, no. 11, Apr. 2022.
[60] S. Mosavat, M. Zella, M. Handte, A. J. Golkowski, and P. J. Marrón, "Experience: Aristotle: wake-up receiver-based, star topology batteryless sensor network," in *Proc. 22nd ACM/IEEE Int. Conf. Inf. Process. in Sensor Netw. (IPSN)*, May 2023, p. 177–190.
[61] M. Grant and S. Boyd, "CVX: Matlab software for disciplined convex programming, version 2.1," http://cvxr.com/cvx, Mar. 2014.

Javier Talavante (Graduate Student Member, IEEE) received the B.S. degree in audiovisual engineering and M.S in telecommunication engineering from Universidad Carlos III de Madrid, Spain, in 2019 and 2021, respectively. He worked at the Infrared Lab in Universidad Carlos III de Madrid. He is currently PhD Candidate at IMDEA Networks, Madrid, Spain. His research interests include optical wireless communications, battery-free devices and embedded systems.

Borja Genovés Guzmán (Senior Member, IEEE) received a Ph.D. degree from Universidad Carlos III de Madrid, Spain, in 2019 (Extraordinary Ph.D. award). He worked as a postdoctoral researcher at IMDEA Networks Institute (Spain) and University of Virginia (USA). He is currently working as a Marie Skłodowska-Curie Actions Postdoctoral Global Fellow in Universidad Carlos III de Madrid and starting as a Ramón y Cajal researcher from September 2025. His research interests are visible light communication (also referred to as LiFi), Internet of Things (IoT) and low-power wireless communications.

Domenico Giustiniano (Senior Member, IEEE) is Research Professor with IMDEA Networks Institute and group leader of the Pervasive Wireless System Group. He also worked for a total of four years in industrial research labs (Disney Research and Telefonica Research). He is leader of the open-source OpenVLC project on visible light communication systems. His current research interests include battery-free IoT systems, unmanned aerial networks and 6G localization.